Plasma Heating and Asymmetric Magnetic Reconnection During Solar Eruptions

Nick Murphy

Harvard-Smithsonian Center for Astrophysics

Collaborators: Paul Cassak, Kelly Korreck, Jun Lin, Mari Paz Miralles, Mitsuo Oka, Crystal Pope, John Raymond, Kathy Reeves, Dan Seaton, Chengcai Shen, Carl Sovinec, Aad van Ballegooijen, David Webb, & Trae Winter

Naval Research Laboratory
April 6, 2012

Introduction

- Understanding astrophysical phenomena requires knowledge of the energy budget
- White light coronagraphs give kinetic energies of CMEs
- The Ultraviolet Coronagraph Spectrometer (UVCS) on SOHO lets us study the thermal energy content of CMEs
- Ionization/recombination timescales are comparable to the CME propagation timescale
- We perform a time-dependent ionization analysis to constrain plasma heating requirements during a CME on 2000 June 28
- We also perform simulations of asymmetric reconnection in flare/CME current sheets
  - Two competing reconnection sites
  - Line-tied asymmetric reconnection

Open Questions

- What are the key characteristics of plasma heating in CMEs?
  - How much are CMEs heated?
  - What causes the heating?
- How does asymmetry modify the reconnection process?
  - Where does the energy go?
  - What are the observational signatures?

We identify six features seen by UVCS in MLSO/MK4 polarization brightness and LASCO white light images

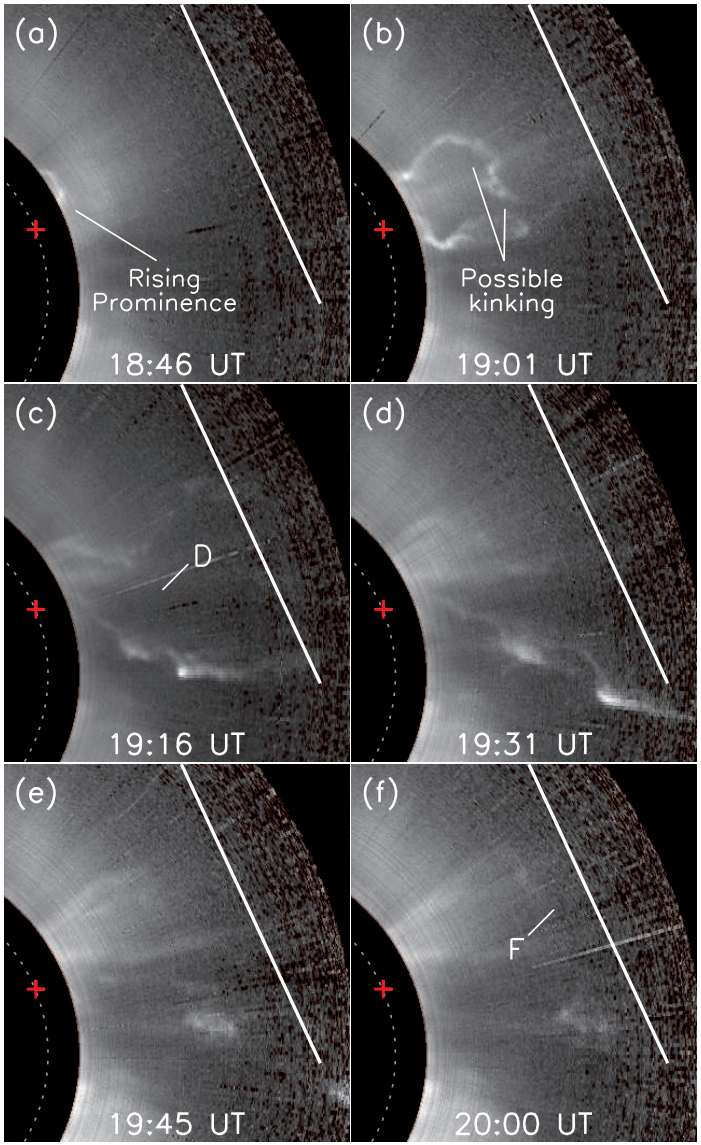

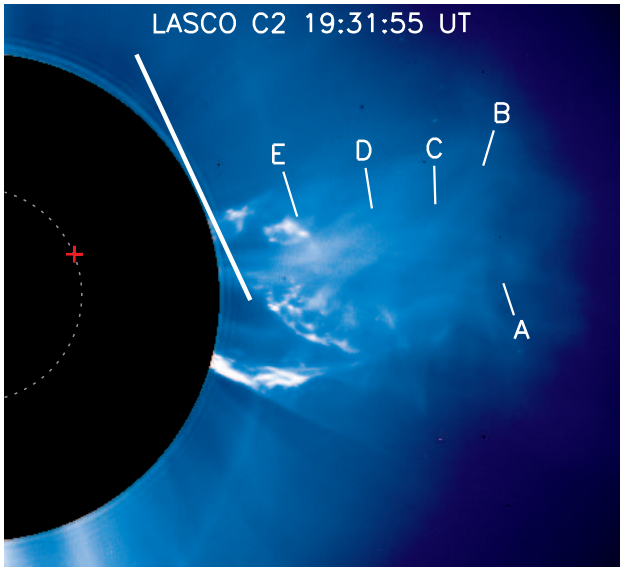

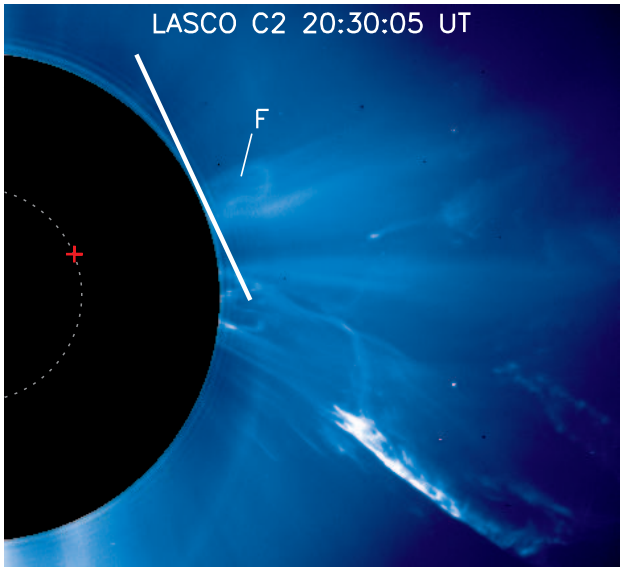

UVCS observed Ly α, Ly β, C III, O V, O VI, C II, and N III emission during this event

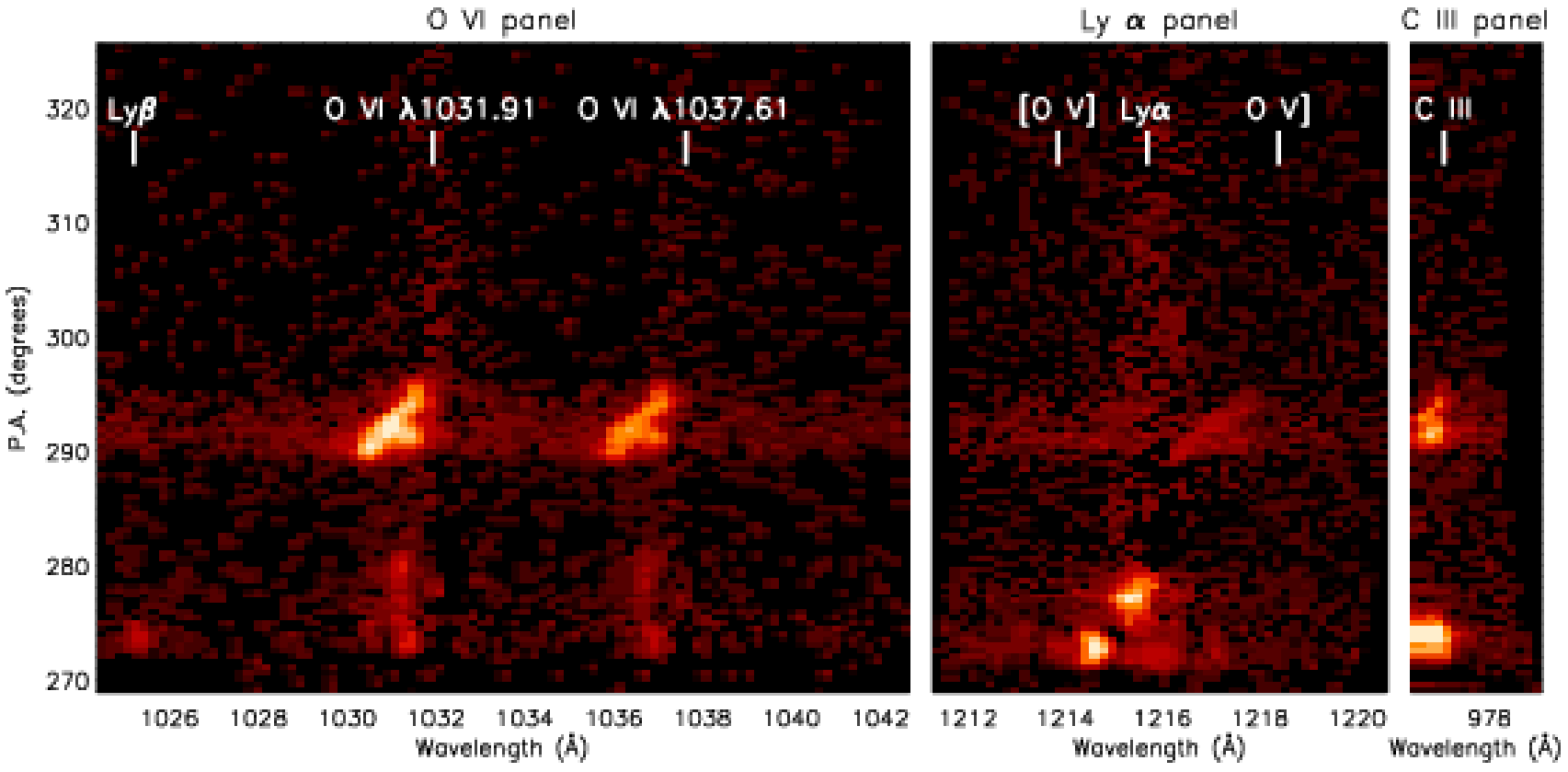

- Blob F appears as a diagonal shear flow feature in UVCS with weak Ly α and Ly β emission

We use a 1-D time-dependent ionization code to track ejecta between the flare site and UVCS slit

- We run a grid of models with different initial densities, initial temperatures, and heating rates (e.g, Akmal et al. 2001)
- The final density is derived from UVCS observations using:
  - The density sensitive [O v]/O v] line ratio
  - Radiative pumping of the O vi doublet (Raymond & Ciaravella 2004)
- Assume homologous expansion
- Multiple heating parameterizations
  - An exponential wave heating model (Allen et al. 1998; AHH)
  - Expanding flux rope model by Kumar & Rust (1996; KR)
  - Heating proportional to n or n^2
- The models consistent with UVCS observations give the allowed range of heating rates
- See Murphy, Raymond, & Korreck (ApJ, 2011)

Allowed temperature histories for blob F

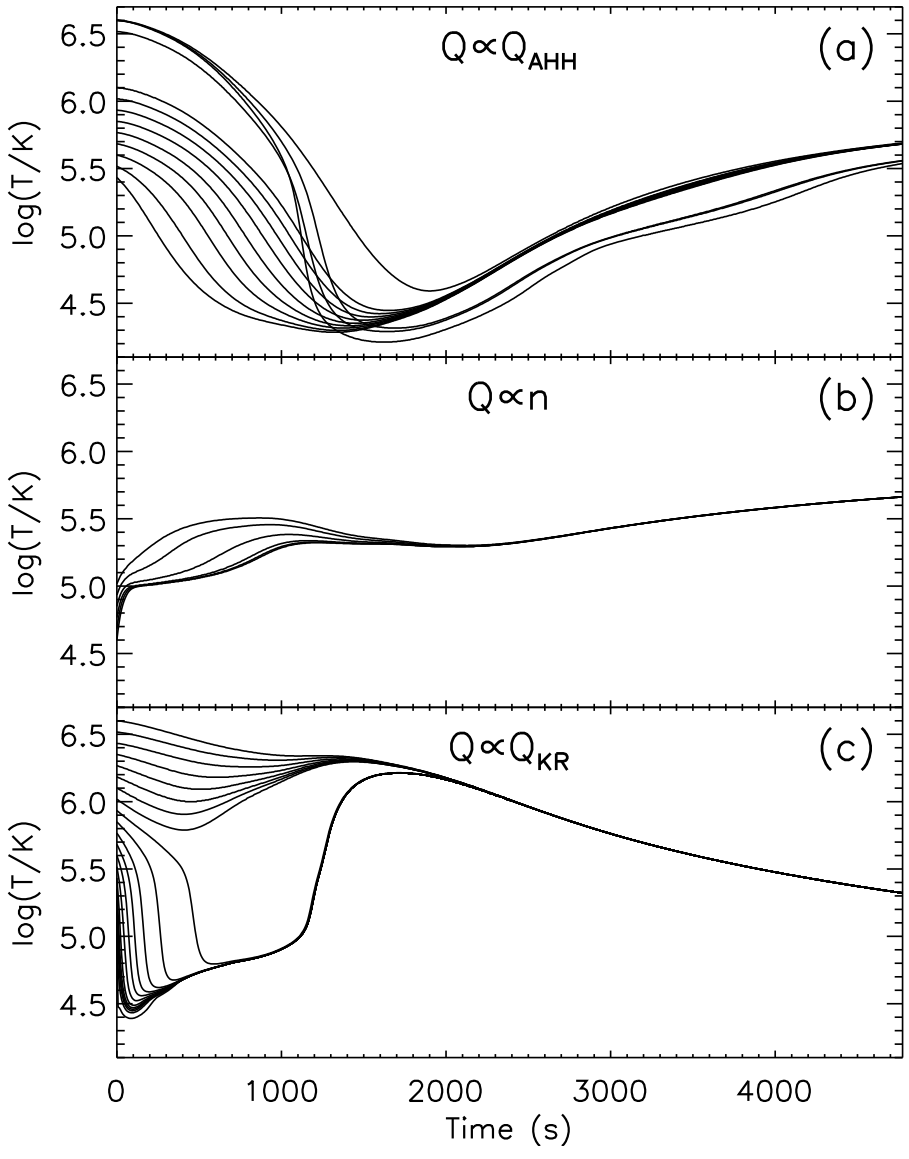

Cumulative heating energy, kinetic energy, and potential energy in units of 10^{14} erg g^{-1}

Blob	$Q_{\rm AHH}$	$Q \propto n$	$Q \propto n^2$	$Q_{\rm KR}$	K.E.	P.E.
A	**6–35**	**7–46**	**22–42**	**7–127**	**136 (>29)**	**7.4**
B	0.3–37	1.4–86	18–117	7–379	164 (>27)	7.9
C	0.2–36	0.6–87	12–112	1–392	164 (>27)	7.7
D	0.2–61	0.4–163	13–112	1–422	136 (>19)	7.9
E	**1.6–13**	**3–13**	**17–109**	**6–30**	**164 (>11)**	**8.2**
F	6.5–8.2	16.9	—	56.6	8.6 (>5.5)	5.5

- For blobs A and E, the cumulative heating energy is less than or comparable to the kinetic energy

Cumulative heating energy, kinetic energy, and potential energy in units of 10^{14} erg g^{-1}

Blob	$Q_{\rm AHH}$	$Q \propto n$	$Q \propto n^2$	$Q_{\rm KR}$	K.E.	P.E.
A	6–35	7–46	22–42	7–127	136 (>29)	7.4
B	**0.3–37**	**1.4–86**	**18–117**	**7–379**	**164 (>27)**	**7.9**
C	**0.2–36**	**0.6–87**	**12–112**	**1–392**	**164 (>27)**	**7.7**
D	**0.2–61**	**0.4–163**	**13–112**	**1–422**	**136 (>19)**	**7.9**
E	1.6–13	3–13	17–109	6–30	164 (>11)	8.2
F	6.5–8.2	16.9	—	56.6	8.6 (>5.5)	5.5

- For blobs B–D, the cumulative heating energy is constrained to be less than ∼2–3 times the kinetic energy

Cumulative heating energy, kinetic energy, and potential energy in units of 10^{14} erg g^{-1}

Blob	$Q_{\rm AHH}$	$Q \propto n$	$Q \propto n^2$	$Q_{\rm KR}$	K.E.	P.E.
A	6–35	7–46	22–42	7–127	136 (>29)	7.4
B	0.3–37	1.4–86	18–117	7–379	164 (>27)	7.9
C	0.2–36	0.6–87	12–112	1–392	164 (>27)	7.7
D	0.2–61	0.4–163	13–112	1–422	136 (>19)	7.9
E	1.6–13	3–13	17–109	6–30	164 (>11)	8.2
F	**6.5–8.2**	**16.9**	—	**56.6**	**8.6 (>5.5)**	**5.5**

- For blob F, the cumulative heating energy is comparable to or greater to the kinetic energy

Candidate mechanisms: wave heating

- Would need $\gtrsim$100 times the wave heating rate of Allen et al. (1998) for coronal holes (e.g., Landi et al. 2010)
- In lab experiments of expanding flux ropes, fast magnetosonic waves generated by the eruption itself heat the plasma (Tripathi et al. 2010)
- Resonant absorption of Alfvén waves is another possibility (Evans et al., submitted)

Candidate mechanisms: small-scale reconnection

- Small-scale reconnection events within the expanding flux rope could heat the plasma (e.g., Kumar & Rust 1996)
- Analogous to Taylor relaxation in an expanding equilibrium
- UVCS measurements limit turbulent energy density
- Role of kink instability?
- Next step: simulate relaxation and reconnection in expanding flux rope

Candidate mechanisms: energetic particles

- Weak, C class flare $\rightarrow$ energetic particle heating unlikely?
- Glesener et al: energetic particles enough to heat event on 2010 Nov 3
- Need to be careful:
  - Non-thermal tail increases ionization rates
  - Are AIA temperature response functions affected?
- Next steps:
  - Quantify effect of energetic particles on ionization rates
  - Simulate hot particle evolution in an expanding flux rope

Candidate mechanisms: CME current sheet upflow

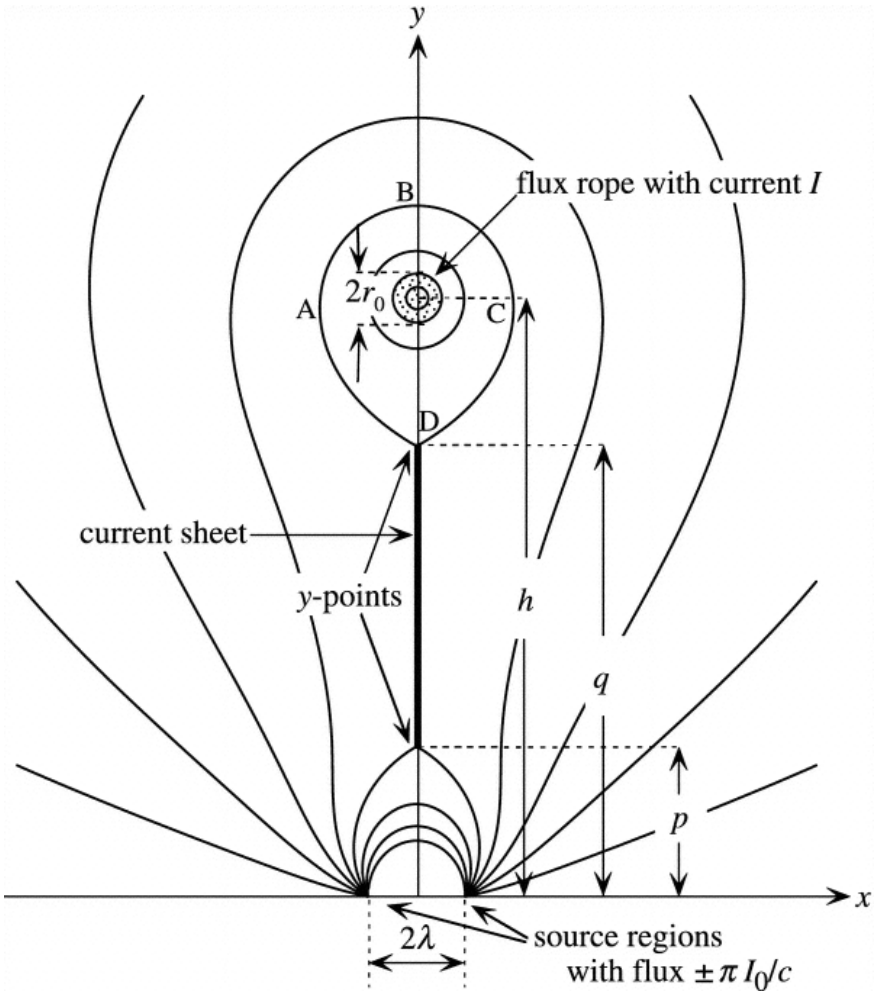

- Flux rope models of CMEs predict the formation of an elongated current sheet behind the rising plasmoid
- Reconnection upflow could heat the ejecta

Open questions

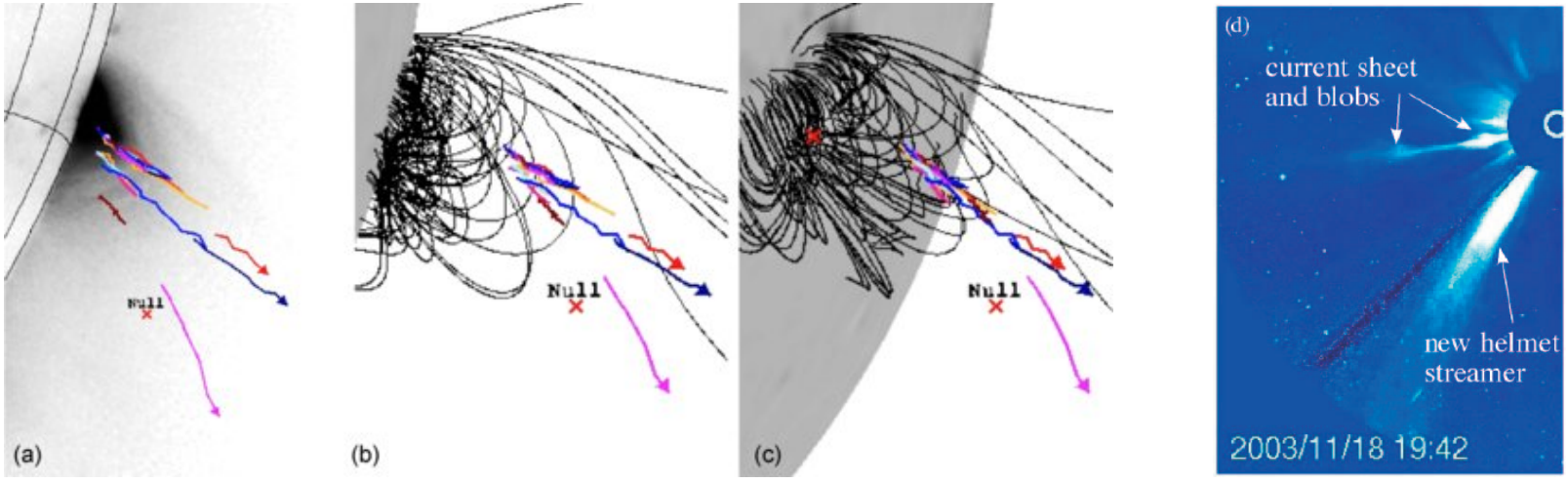

- Are post-eruption current sheets actively reconnecting?
- Are these current sheets energetically important to the eruption as a whole?
- Where is the principal X-line? $\Longleftrightarrow$ Where does the energy go?
- Are CME CSs responsible for mass input and plasma heating in CMEs?
- Are large-scale blobs due to the plasmoid instability?
  - Perhaps, but some show C III and other cool lines

We perform resistive MHD simulations of two initial X-lines which retreat from each other as reconnection develops (Murphy 2010)

- The 2-D simulations start from a periodic Harris sheet which is perturbed at two nearby locations ($x = \pm 1$)
- Use the NIMROD extended MHD code (Sovinec et al. 2004)
- Domain: $-30 \leq x \leq 30$, $-12 \leq z \leq 12$
- Simulation parameters: $\eta = 10^{-3}$, $\beta_\infty = 1$, $\mathrm{S} = 10^3$–10^4, $\mathrm{Pm} = 1$, $\gamma = 5/3$, $\delta_0 = 0.1$
- Define:
  - x_n is the position of the X-line
  - x_s is the position of the flow stagnation point
  - $V_x(x_n)$ is the velocity *at* the X-line
  - $\frac{\mathrm{d}x_n}{\mathrm{d}t}$ is the velocity *of* the X-line
- $\hat{\mathbf{x}}$ is the outflow direction, $\hat{\mathbf{y}}$ is the out-of-plane direction, and $\hat{\mathbf{z}}$ is the inflow direction
- We show only $x \geq 0$ since the simulation is symmetric

The CSs have characteristic single wedge shapes

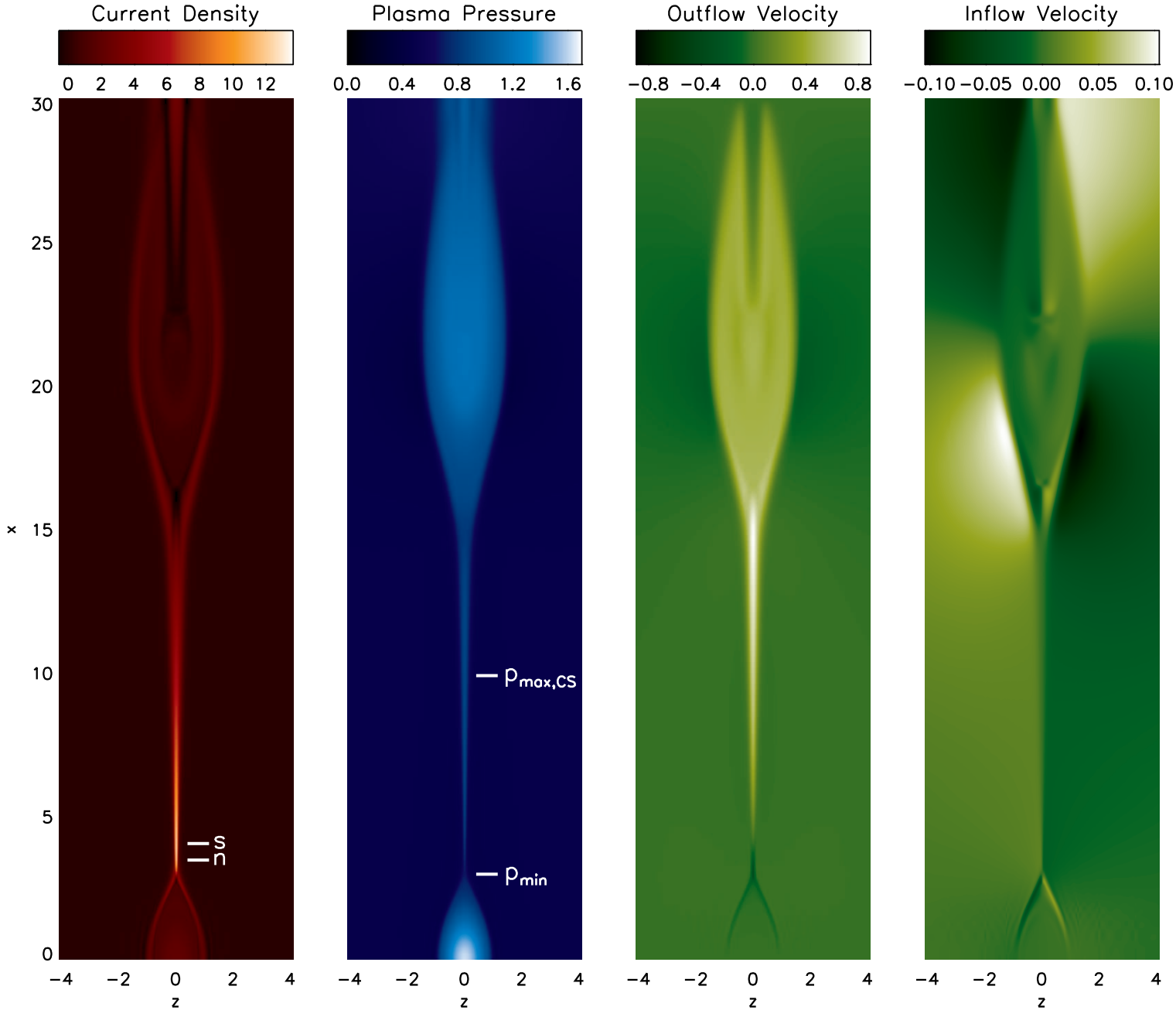

The flow stagnation point and X-line are not colocated

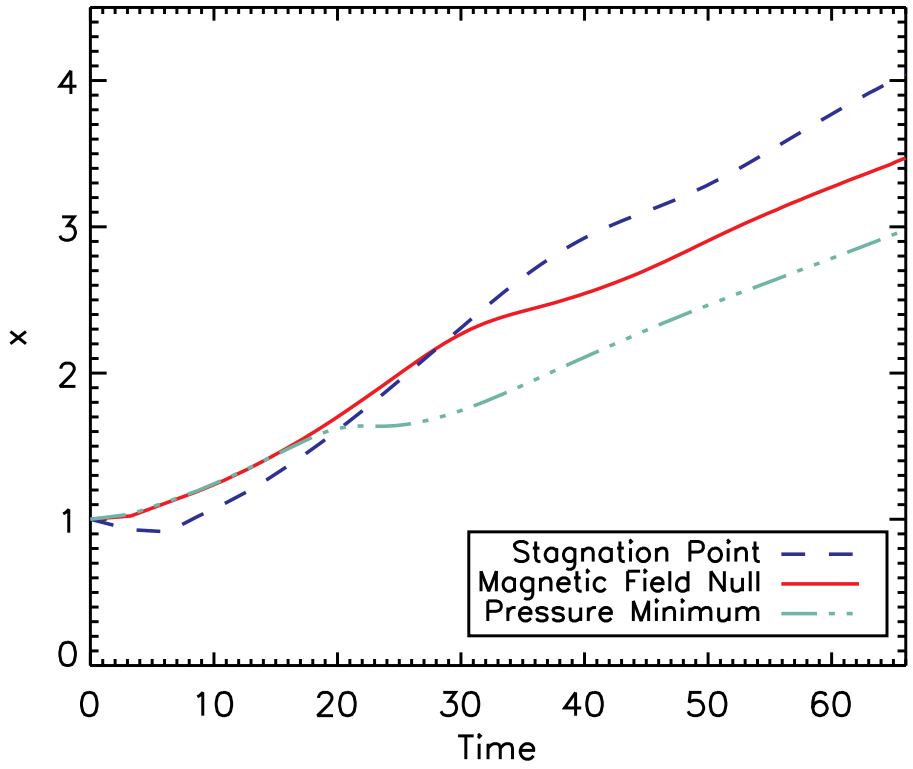

- Surprisingly, the relative positions of the X-line and flow stagnation point switch!
- This occurs so that the stagnation point will be located near where the tension and pressure forces cancel
- Reconnection develops slowly because the X-line is located near a pressure minimum early in time

Late in time, the X-line diffuses against strong plasma flow

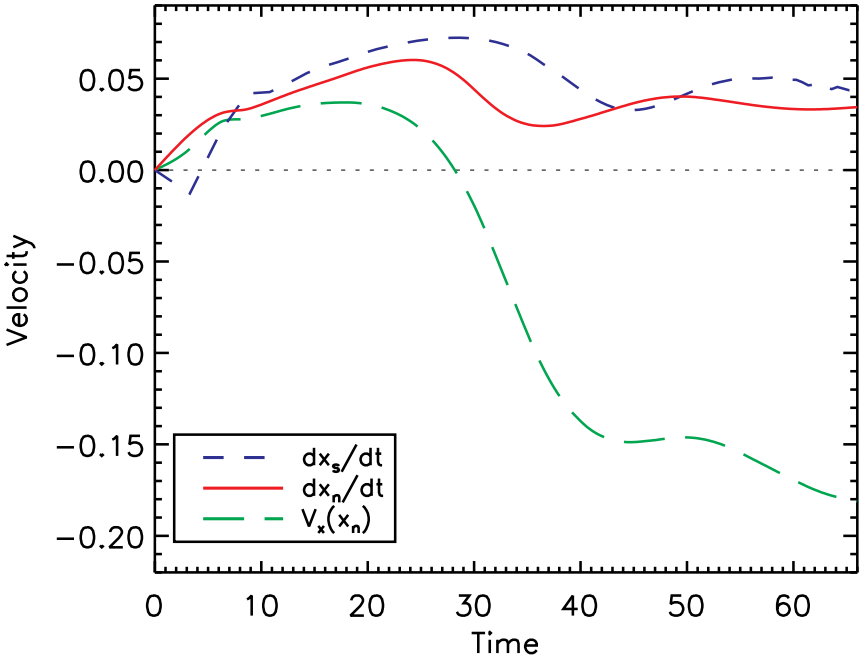

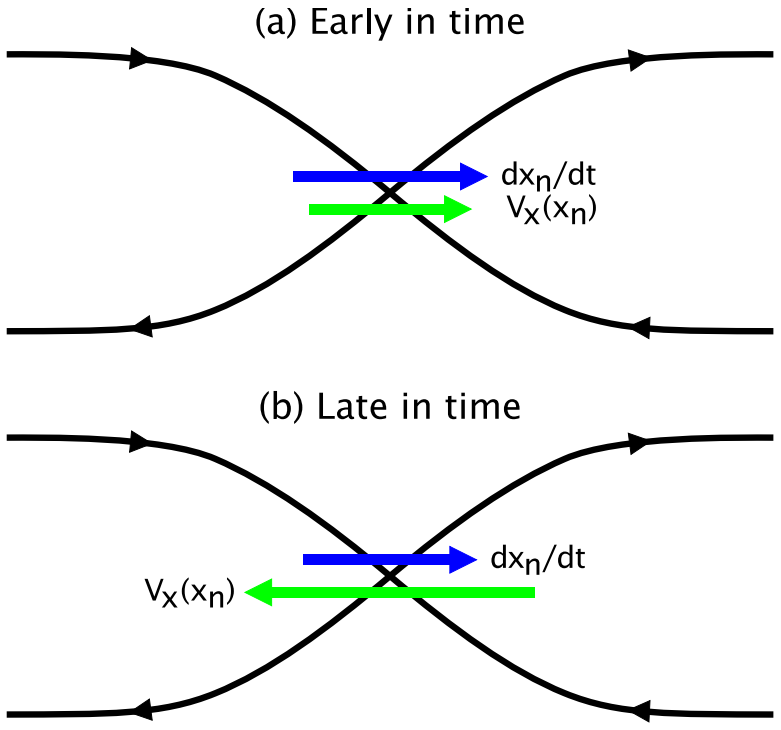

- The stagnation point retreats more quickly than the X-line
- Any difference between $\frac{\mathrm{d}x_n}{\mathrm{d}t}$ and $V_x(x_n)$ must be due to diffusion (e.g., Seaton 2008, Murphy 2010)
- The velocity *at* the X-line is not the velocity *of* the X-line!

The X-line moves in the direction of increasing total reconnection electric field strength

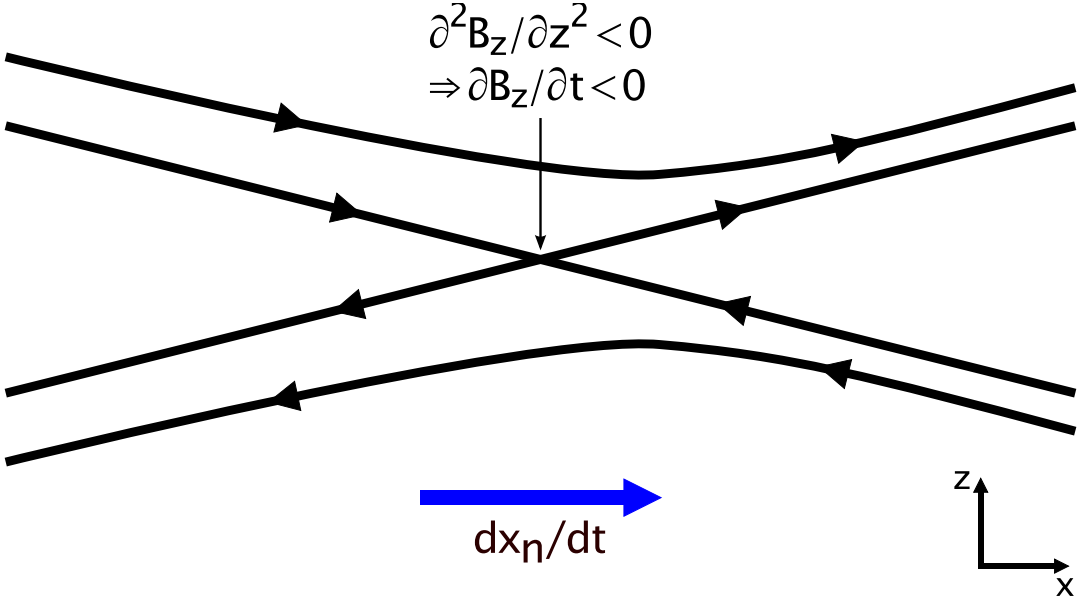

- X-line retreat occurs through a combination of:
  - Advection by the bulk plasma flow
  - Diffusion of the normal component of the magnetic field
- X-line motion depends intrinsically on local parameters evaluated at the X-line
  - X-lines are not (directly) pushed by pressure gradients

Next: we consider line-tied reconnection between magnetic fields of different strengths

- Reconnecting magnetic fields are asymmetric:

$$B_y(x) = \frac{B_0}{1+b} \tanh\left(\frac{x}{\delta_0} - b\right) \tag{1}$$

- $-7 \leq x \leq 7$, $0 \leq y \leq 30$; conducting wall BCs
  - High resolution needed over a much larger area
- Magnetic field ratios: 1.0, 0.5, 0.25, and 0.125
- $\beta_0 = 0.18$ in higher magnetic field upstream region
- Caveats: 1-D initial equilibrium, outer conducting wall BCs, and we do not consider the rising flux rope in detail

Reconnection with both asymmetric inflow and outflow

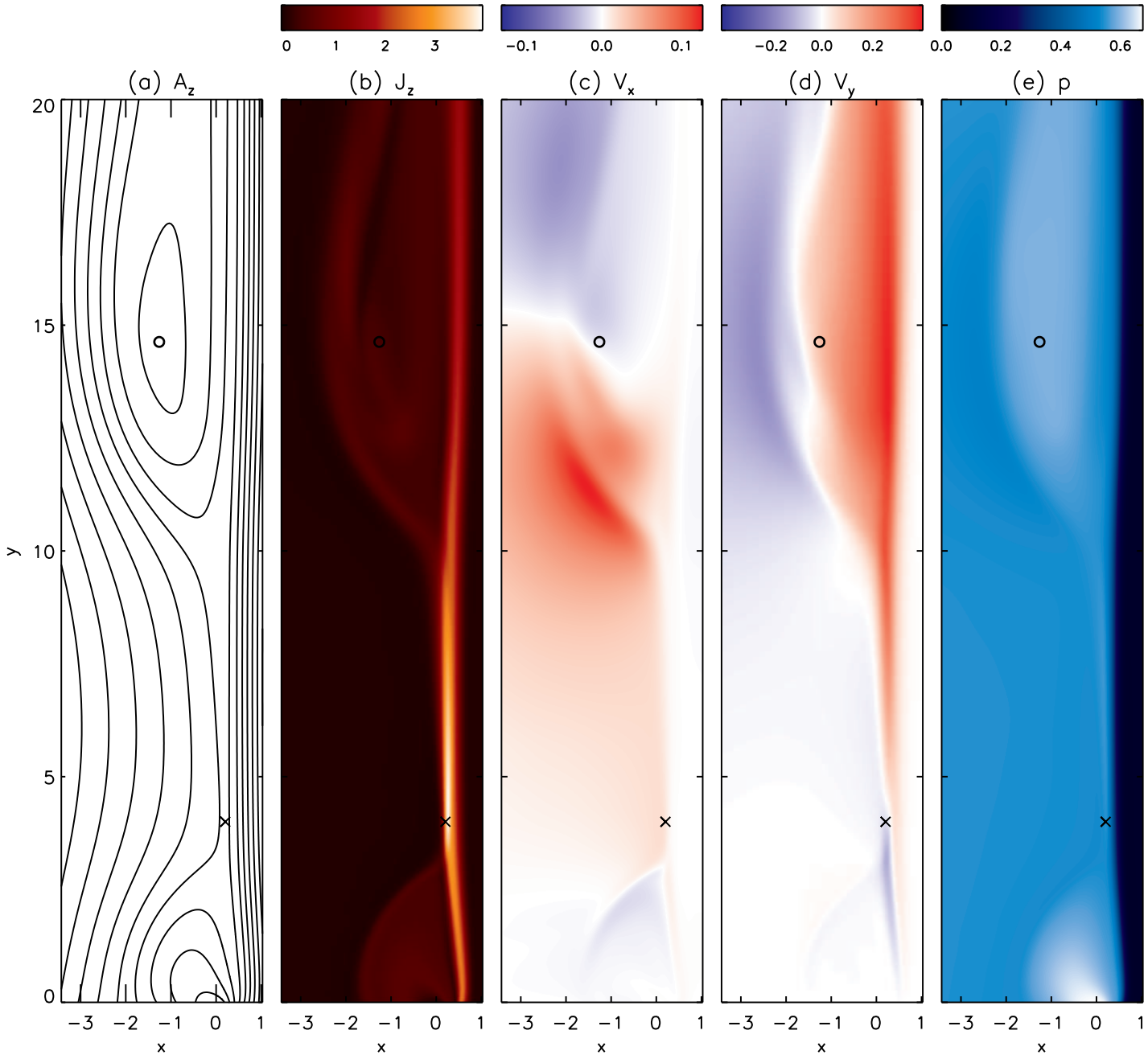

Again, the plasma velocity at the X-line differs greatly from the rate of X-line motion

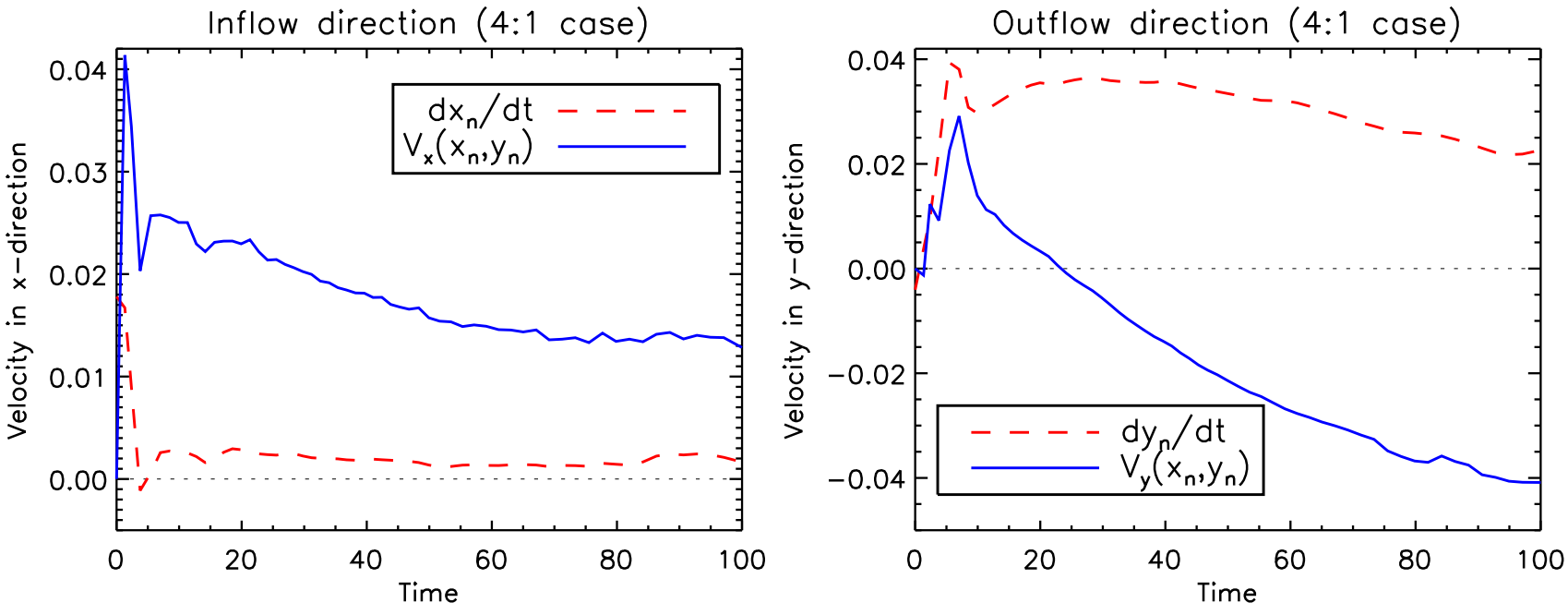

- $V_x(x_n, y_n)$ and $V_y(x_n, y_n)$ give the velocity at the X-line
- $\mathrm{d}x_n/\mathrm{d}t$ and $\mathrm{d}y_n/\mathrm{d}t$ give the rate of X-line motion
- No flow stagnation point within the CS

The post-flare loops develop a characteristic candle flame structure

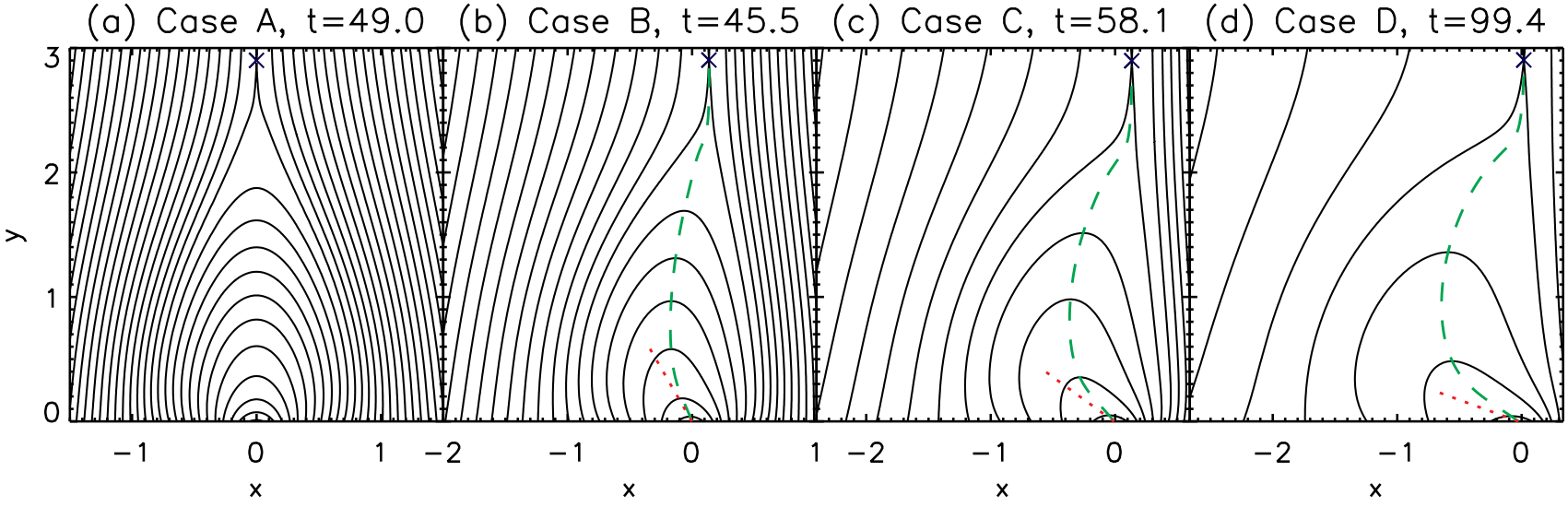

- Magnetic flux contours for $B_L/B_R \in \{1,\ 0.5,\ 0.25,\ 0.125\}$ when $y_n \approx 2.9$
- Dashed green line: loop-top positions
- Dotted red line: analytic asymptotic approximation

The Tsuneta (1996) flare is a famous candidate event

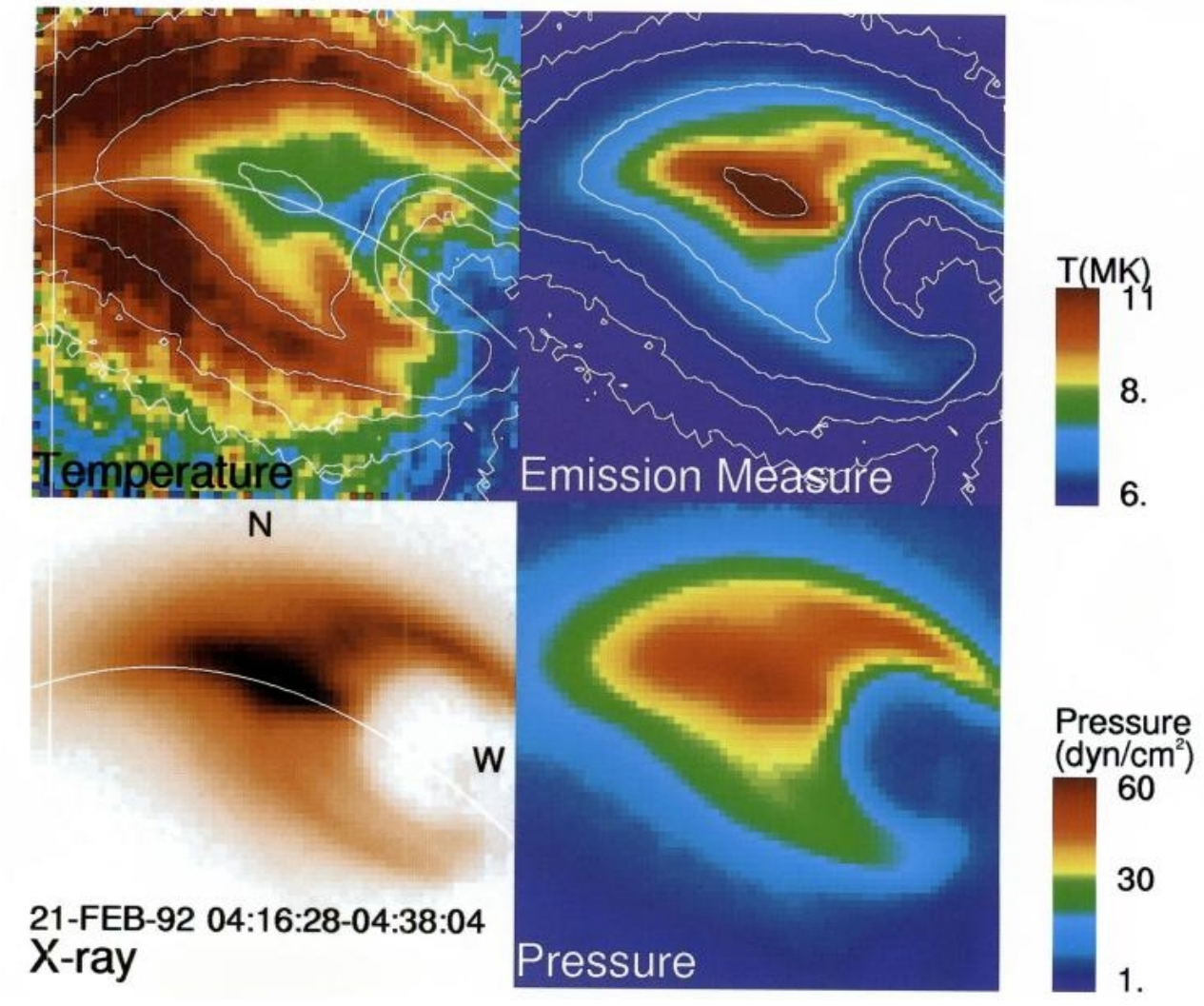

- Shape suggests north is weak **B** side

Asymmetric speeds of footpoint motion

- In two-dimensional models, the footpoints of newly reconnected loops move away from each other as more flux is reconnected
- In two-dimensions, the amount of flux reconnected on each side of the loop must be equal to each other
- When the magnetic fields are asymmetric, the footpoint on the strong **B** side will move slowly compared to the footpoint on the weak **B** side
- Because of the patchy distribution of flux on the photosphere, more complicated motions frequently occur (e.g., Bogachev et al. 2005; Grigis & Benz 2005; Su et al. 2007; Yang et al. 2009)

Asymmetric hard X-ray (HXR) footpoint emission

- The standard model of flares predicts HXR emission at the flare footpoints from energetic particles (EPs) impacting the chromosphere
- Magnetic mirroring reflects energetic particles (EPs) preferentially on the strong **B** side
- More particles should escape on the weak **B** side, leading to greater HXR emission
- This trend is observed in $\sim 2/3$ of events (Goff et al. 2004)
  - Additional factors include:
    - Asymmetry in initial pitch angle distributions of EPs
    - Directionality of the reconnecting electric field (Hamilton et al. 2005; Li & Lin, accepted)
    - Different column densities (cf. Saint-Hilaire et al. 2008)
  - More detailed energetic particle modeling is required

The outflow plasmoid develops net vorticity because the CS outflow impacts it at an angle

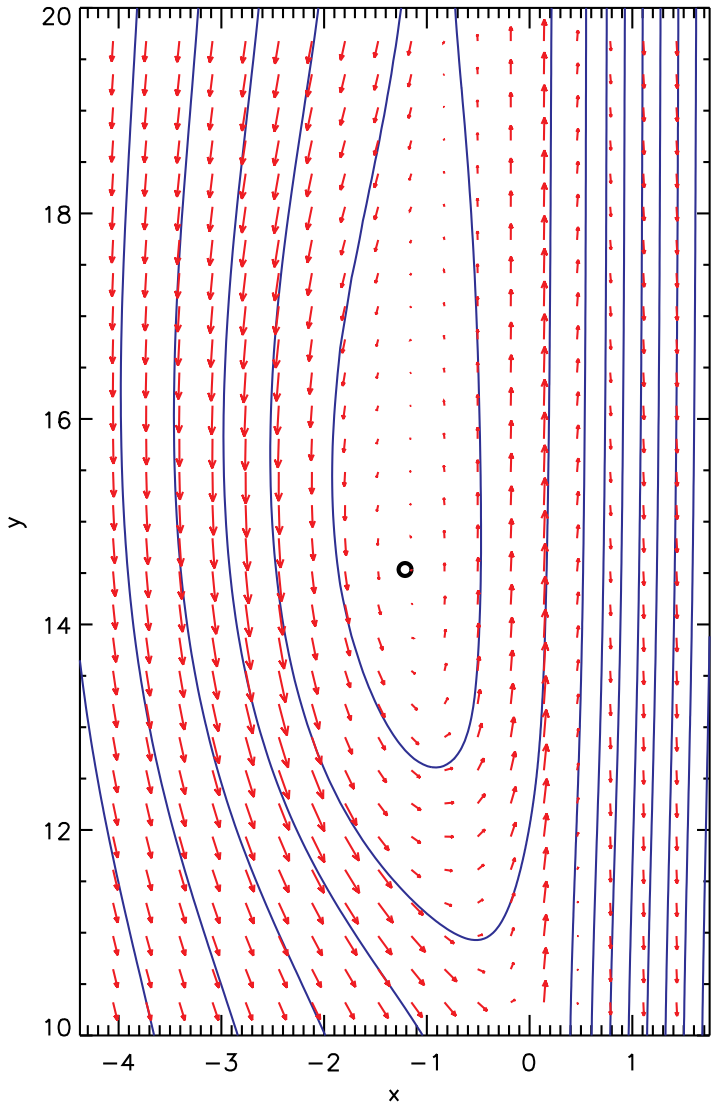

- Velocity vectors in reference frame of O-point

Conclusions

- Heating is an important but not well understood term in the CME energy budget
- For some features the plasma heating is comparable to or greater than the kinetic energy
- Candidate heating mechanisms include the CME current sheet, small-scale reconnection, energetic particles and dissipation of waves driven by the eruption
- X-line retreat is due to advection by the bulk plasma flow and diffusion of the normal component of the magnetic field
- Observational signatures of line-tied asymmetric reconnection include
  - Skewed candle flame shape of post-flare loops
  - Strong magnetic field footpoint moves less quickly (flux conservation) and has less hard X-ray emission (mirroring)
  - Circulation in rising flux rope

Extra Slides

What sets the rate of X-line retreat?

- The inflow (z) component of Faraday's law for the 2D symmetric inflow case is

$$\frac{\partial B_z}{\partial t} = -\frac{\partial E_y}{\partial x} \tag{2}$$

- The convective derivative of B_z at the X-line taken at the velocity of X-line retreat, $\mathrm{d}x_n/\mathrm{d}t$, is

$$\left.\frac{\partial B_z}{\partial t}\right|_{x_n} + \frac{\mathrm{d}x_n}{\mathrm{d}t}\left.\frac{\partial B_z}{\partial x}\right|_{x_n} = 0 \tag{3}$$

The RHS of Eq. (3) is zero because $B_z(x_n, z = 0) = 0$ by definition for this geometry.

Deriving an exact expression for the rate of X-line retreat

- From Eqs. 2 and 3:

$$\frac{\mathrm{d}x_n}{\mathrm{d}t} = \left.\frac{\partial E_y/\partial x}{\partial B_z/\partial x}\right|_{x_n} \tag{4}$$

- Using $\mathbf{E} + \mathbf{V} \times \mathbf{B} = \eta \mathbf{J}$, we arrive at

$$\frac{\mathrm{d}x_n}{\mathrm{d}t} = V_x(x_n) - \eta \left[\frac{\frac{\partial^2 B_z}{\partial x^2} + \frac{\partial^2 B_z}{\partial z^2}}{\frac{\partial B_z}{\partial x}}\right]_{x_n} \tag{5}$$

- $\frac{\partial^2 B_z}{\partial z^2} \gg \frac{\partial^2 B_z}{\partial x^2}$, so X-line retreat is caused by diffusion of the normal component of the magnetic field along the inflow direction
- This result can be extended to 3D nulls and to include additional terms in the generalized Ohm's law